# We are IntechOpen, the world's leading publisher of Open Access books Built by scientists, for scientists

**4,800**
Open access books available

**122,000**
International authors and editors

**135M**
Downloads

Our authors are among the

**154**
Countries delivered to

**TOP 1%**
most cited scientists

**12.2%**
Contributors from top 500 universities

CLARIVATE ANALYTICS BOOK CITATION INDEX INDEXED

WEB OF SCIENCE™

Selection of our books indexed in the Book Citation Index in Web of Science™ Core Collection (BKCI)

## Interested in publishing with us?
## Contact book.department@intechopen.com

Numbers displayed above are based on latest data collected.
For more information visit www.intechopen.com

14

# Ferroelectric Field Effect Control of Magnetism in Multiferroic Heterostructures

Carlos A. F. Vaz[1] and Charles H. Ahn[2]
[1]*SwissFEL, Paul Scherrer Institut, Villigen PSI*
[2]*Department of Applied Physics, Yale University, New Haven, Connecticut*
[1]*Switzerland*
[2]*U.S.A.*

## 1. Introduction

Nanotechnology stands for a new paradigm in materials science that aims at exploring and controlling new physical phenomena and enhanced functionalities that emerge at the nanoscale. These opportunities are a direct consequence of reduced dimensionality and/or interfacial phenomena from proximity effects between dissimilar materials Zubko et al. (2011). Progress in growth techniques Chambers (2010); Eckstein & Bozovic (1995); Martin et al. (2010); McKee et al. (1998); Posadas et al. (2007); Reiner et al. (2009); Schlom et al. (1992); Vaz et al. (2009a); Vrejoiu et al. (2008), nanoscale characterization tools Zhu (2005), and first principles calculations Cohen (2000); Fennie (2008); Picozzi & Ederer (2009); Rabe & Ghosez (2007); Spaldin & Pickett (2003); Waghmare & Rabe (2005) have been instrumental to our present ability to control matter down to the atomic scale and to fabricate nanoscale device structures with the potential for technological applications. Examples of current research work that aims at addressing some of the current grand challenges include the search for ultrasensitive sensors and actuators for applications in areas such as medicine and energy harvesting, the development of smaller and more energy efficient electronic devices that could replace current CMOS switches, and the design of intelligent systems that incorporate complex operations at the core processing level. While the approach employed to date has relied on building up complexity from basic building blocks (e.g., complex microprocessor units formed of MOSFET devices), a new approach is being developed that directly explores the complex state of matter to achieve integrated functionalities and more complex operations at a fundamental level. Key to this effort has been the sustained research work aimed at understanding the properties of strongly correlated systems, and at controlling such properties down to the atomic scale, from a device physics perspective.

In this context, a particularly interesting class of materials are so-called *multiferroic* systems, which are characterized by the presence of simultaneous magnetic and ferroelectric order. As such, they offer the possibility of achieving control of the magnetic state via applied electric fields, or vice versa, which could find applications in ultrasensitive magnetic sensors and transducers, solid state transformers, magnetoelectrooptic devices, energy harvesting and storage, and new spin-based logic devices in the context of *spintronics* Bibes & Barthélémy (2007); Cibert et al. (2005); Žutić et al. (2004). In most single phase multiferroic materials, the origin of magnetic and ferroelectric orders is largely independent, with the consequence that the coupling between magnetism and ferroelectricity (mediated by the spin-orbit coupling)

is weak; in those instances where the coupling is strong, the critical temperatures tend to be small Khomskii (2006; 2009); Picozzi & Ederer (2009). To overcome the weak magnetoelectric coupling of single-phase multiferroic materials, alternate approaches have been developed that explore proximity and interfacial effects between magnetic and ferroelectric materials to form composite structures with enhanced coupling between electric and magnetic properties. By judiciously engineering the interfacial properties at the nanoscale, a strong coupling between magnetic and ferroelectric order parameters can be achieved. This new class of artificially structured composite materials exhibits magnetoelectric couplings that are orders of magnitude larger that those typical of single-phase, intrinsic multiferroics Fiebig (2005); Ma et al. (2011); Vaz et al. (2010a).

An example of the promise afforded by this approach is provided by the particular case of the multiferroic perovskite $BiFeO_3$, characterized by magnetic and ferroelectric critical temperatures well above room temperature ($T_c^{\mathrm{m}} = 643$ K and $T_c^{\mathrm{e}} = 1100$ K, respectively) Catalan & Scott (2009). $BiFeO_3$ has generated much interest recently, following the first report of the growth of epitaxial thin films Wang et al. (2003) and the demonstration of very large electric polarizations in high quality single crystalline films and in bulk crystals Lebeugle et al. (2007); Shvartsman et al. (2007); Wang et al. (2003). In this system, ferroelectricity originates from the lone-pair active Bi cations Neaton et al. (2005); Ravindran et al. (2006), while the magnetic order originates from the oxygen-mediated superexchange interaction between the Fe cations, which favors an antiferromagnetic coupling between nearest neighbor spins Kiselev et al. (1963). The magnetic state is modified further by a break in center of symmetry and the presence of a ferroelectric polarization, which gives rise to a local spin canting between the two spin sublattices (and to a weak magnetic moment) through the Dzyaloshinskii-Moriya interaction Dzialoshinshkii (1957); Moriya (1960). In addition, the coupling of the polarization to gradients of the magnetization leads to an inhomogeneous spin configuration characterized by an incommensurate rotation of the total local spin along a $\langle 10\bar{1}\rangle_{\mathrm{pc}}$ direction (indexed to the pseudocubic perovskite structure) and lying in the $\{1\bar{2}1\}_{\mathrm{pc}}$ plane, defined by the cycloid propagation direction and the electric polarization (with easy axes along $\langle 111\rangle_{\mathrm{pc}}$), with a period of about 62 nm (*spin cycloid*) Catalan & Scott (2009); Picozzi & Ederer (2009); Sosnowska et al. (1982). This spin cycloid averages out the magnetic moment and leads to a vanishing linear magnetoelectric coupling and to a small effective magnetoelectric response; however, at the nanoscale, there is a strong coupling between the electric polarization and the magnetic spins, since they are constrained to point perpendicular to each other, indicating that a change in the orientation of the electric polarization will result in a change in the spin direction Cazayous et al. (2008); Lebeugle et al. (2008). Such a phenomenon has been demonstrated experimentally Lee et al. (2008); Zheng et al. (2006) and has been explored in exchange-bias coupled multiferroic heterostructures to change the magnetization direction of a ferromagnetic layer exchange-coupled to the $BiFeO_3$ Chu et al. (2008); Wu et al. (2010). This approach to magnetoelectric coupling illustrates the current trend towards engineering larger magnetoelectric couplings by relying on interfacial effects between different materials, an approach that can be traced back to the 1970s, when the first attempts to grow strain-mediated ferroelectric-ferromagnetic composites were made van Suchtelen (1972). In fact, the most common approach to date for achieving a magnetoelectric coupling in composites relies on strain to mediate the magnetic and electrical properties by inducing crystal deformations on either the magnetic phase through the converse piezoelectric effect, or in the ferroelectric phase through magnetostriction Fiebig (2005); Ma et al. (2011); Ramesh & Spaldin (2007); Thiele et al. (2007); Vaz et al. (2009b; 2010a). The effect is indirect, but can be optimized to yield large magnetoelectric responses by a suitable choice of the material components and device geometry Nan et al. (2008); Srinivasan (2010); Wang et al. (2009). Another promising route

involves a direct, charge-mediated magnetoelectric coupling in ferroelectric/ferromagnetic oxide composite multiferroic heterostructures, where the spin state of the magnetic oxide is controlled via charge doping induced by the electric polarization of a ferroelectric Molegraaf et al. (2009); Vaz et al. (2010b). For $Pb(Zr_{0.2}Ti_{0.8})O_3/La_{0.8}Sr_{0.2}MnO_3$ (PZT/LSMO) heterostructures, the effect is electronic in origin and results from a change in the magnetic spin configuration as a function of the ferroelectric polarization direction, demonstrating electric field control of magnetism in this system (Section 3).

In this chapter, we consider the recent developments in the electric field control of magnetism in artificial heterostructures based on electrostatic doping. This approach has been explored in various systems, including dilute magnetic semiconductors, transition metals, and complex oxides; an overview of the work carried out in each of these systems is given in Section 2. The focus will be on complex oxide heterostructures, and in particular on our recent work demonstrating a strong magnetoelectric coupling in PZT/LSMO multiferroic heterostructures (Section 3). Due to strong electron correlations, complex oxides offer an inexhaustible range of possibilities for the study of novel phenomena that arise from the sensitivity of these materials to charge, strain, electric and magnetic fields, among other control parameters, with the attendant promise for device applications Imada et al. (1998); Tokura (2006); Tokura & Nagaosa (2000).

## 2. Electrostatic control of magnetism in artificial heterostructures

One approach to artificial multiferroic structures exploits the electric field effect to achieve an electrostatic modification of the charge carrier density and to induce changes in the magnetic state. The working concept is similar to that of a field effect transistor, where an induced or spontaneous electric polarization at the gate dielectric interface is screened by charge carriers from the channel layer, leading to charge accumulation or depletion over a thickness determined by the screening length of the material. In materials where the magnetic properties are intimately linked to charge, a change in carrier doping results in a change in the magnetic properties. The amount of charge carrier modulation required will depend on the particular system. For strongly correlated oxides, where typical carrier densities are of the order of $10^{21}$ $cm^{-3}$, the requisite modulation in the charge carrier doping can be achieved by using a ferroelectric for the gate dielectric, an approach termed the *ferroelectric field effect* Ahn et al. (2006); Venkatesan et al. (2007). In this approach to electrostatic doping, the charge carriers screen the large surface bound charge of the ferroelectric; for a ferroelectric such as $Pb(Zr,Ti)O_3$ (PZT), the charge carrier modulation is of the order of $10^{14}$ $cm^{-2}$, much larger than is possible to attain using silicon oxide as the gate dielectric Ahn et al. (2003). The field effect approach has been explored to control a variety of properties in complex systems, including superconductivity Ahn et al. (1999); Caviglia et al. (2008); Frey et al. (1995); Parendo et al. (2005); R. E. Glover & Sherrill (1960); Talyansky et al. (1996) and metal-insulator transitions Dhoot et al. (2009); Hong et al. (2005; 2003). Ferroelectric gates have also been proposed for non-volatile field effect transistors (FET), where the on/off states are maintained by the ferroelectric polarization Brown (1957); Looney (1957); Miller & McWhorter (1992); Park et al. (2003). Electrostatic control of magnetism has been reported in the last decade for a variety of systems, including dilute magnetic semiconductors (DMS), transition metal ferromagnets, and complex oxides, as discussed briefly below.

The phenomenology of the magnetoelectric coupling in materials has been discussed extensively, and we refer to a recent review for details and for the relevant literature Vaz et al. (2010a). The figure of merit that characterizes the coupling between the electric and magnetic order parameters is the magnetoelectric susceptibility, which measures the change in magnetic

moment for a given applied electric field. In the case where the magnetoelectric response is linear, the magnetoelectric susceptibility $\alpha = \mu_0 dM/dE_0$ (in S.I., where $\mu_0$ is the permeability of vacuum, $M$ is the magnetization, and $E_0$ is the external applied electric field) is well defined, but it is less so in the more general case where the magnetoelectric response is non-linear. In such instances, it is common to define an effective magnetoelectric constant corresponding to the change in magnetization for a given applied electric field (or conversely, the change in electric polarization for a given applied magnetic field). In composite systems relying on interfacial effects, it is useful to define a surface (interface) magnetoelectric coefficient $\alpha_s$, corresponding to the change in surface magnetization for a given applied electric field Duan et al. (2008); Fechner et al. (2008); Niranjan et al. (2009). With the definition given above, the linear magnetoelectric constant has units of s $m^{-1}$ in S.I. units, while in cgs units it is dimensionless Rivera (1994); they are related one to the other by the speed of light in vacuum, such that a dimensionless relative magnetoelectric constant ($\alpha_r$) independent of the system of units can be defined, in analogy with the magnetic and electric relative permitivities Hehl et al. (2008; 2009). Often, however, $\alpha$ is given in mixed units, such as Oe cm $V^{-1}$. We list in Table 1 the magnetoelectric response of charge-mediated multiferroic heterostructures reported in the literature, both in terms of the interfacial and relative magnetoelectric coupling coefficients.

| System | $10^3\alpha$ | $10^{12}\alpha_s$ | $\alpha_r$ | $T$ (K) | Reference |
|---|---|---|---|---|---|
| bcc Fe(001) | 0.002 | 0.024 | 0.0005 | Theory | Duan et al. (2008) |
| hcp Co(0001) | 0.0008 | 0.016 | 0.0002 | Theory | Duan et al. (2008) |
| fcc Ni(001) | 0.002 | 0.03 | 0.0005 | Theory | Duan et al. (2008) |
| 9 ML Fe/MgO | 0.008 | 0.11 | 0.0023 | Theory | Niranjan et al. (2010) |
| 2 ML Fe/$BaTiO_3$ | 10 | 200 | 3.0 | Theory | Duan et al. (2006) |
| 1 ML Fe/$BaTiO_3$ | 16 | 230 | 4.8 | Theory | Fechner et al. (2008) |
| Fe/$BaTiO_3$/Pt | 3 | 43 | 0.9 | Theory | Cai et al. (2009) |
| 1 ML Fe/$PbTiO_3$ | 73 | 1000 | 22 | Theory | Fechner et al. (2008) |
| Ni/$BaTiO_3$/Pt | 15 | 260 | 4.5 | Theory | Cai et al. (2009) |
| hcp Co/$BaTiO_3$/Pt | 4 | 81 | 1.2 | Theory | Cai et al. (2009) |
| $CrO_2$/$BaTiO_3$/Pt | 10 | 150 | 3.0 | Theory | Cai et al. (2009) |
| $Fe_3O_4$/$BaTiO_3$ | 20 | 200 | 5.7 | Theory | Niranjan et al. (2008) |
| $SrRuO_3$/$SrTiO_3$ | 0.05 | 2 | 0.015 | Theory | Rondinelli et al. (2008) |
| $SrRuO_3$/$BaTiO_3$ | 1.1 | 42 | 0.32 | Theory | Rondinelli et al. (2008) |
| $SrRuO_3$/$BaTiO_3$ | 5.9 | 230 | 1.8 | Theory | Niranjan et al. (2009) |
| PZT/LSMO ($x = 0.2$) | 0.8 | 310 | 2.4 | 100 K | Molegraaf et al. (2009) |
| PZT/LSMO ($x = 0.2$) | 6.2 | 2900 | 22 | 100 K | Vaz et al. (2010b;c) |
| PZT/LSMO ($x = 0.2$) | –13.5 | –6300 | –49 | 180 K | Vaz et al. (2010c) |

Table 1. Values of the magnetoelectric coupling coefficient reported in the literature for charge-driven multiferroic heterostructures. $\alpha$ is given in units of Oe cm $V^{-1}$, $\alpha_s$ in units of Oe $cm^2$ $V^{-1}$; $T$ is the temperature. When not directly provided, the surface magnetoelectric coupling coefficient $\alpha_s$ is estimated by multiplying $\alpha$ by 1 ML of the corresponding magnetic material; for the case of the PZT/LSMO structures, $\alpha_s$ and $\alpha_r$ are estimated by multiplying the experimental value of $\alpha$ by the LSMO film thickness.

The nature of the magnetoelectric effect due to charge screening can be distinguished between (i) enhanced spin imbalance at the Fermi level due to screening and the corresponding modification in the magnetic moment of the system as a function of the electric field Zhang (1999); (ii) changes in magnetic moment due to changes in electronic bonding at the polarized

dielectric interface Duan et al. (2006); (iii) changes in the magnetic order with the charge density Gerhard et al. (2010); Kudasov & Korshunov (2007); Ovchinnikov & Wang (2008); Sun et al. (2010); Vaz et al. (2010b), whereby the magnetic state of the system is modified due to changes in the charge carrier density, either between magnetic and non-magnetic states, or between states with different magnetic spin configurations; and (iv) changes in the magnetic anisotropy that lead to different global magnetic states for different applied electric fields Maruyama et al. (2009); Niranjan et al. (2010).

### 2.1 Electrostatic control of magnetism in dilute magnetic semiconductors

The field effect approach to controlling magnetism is well suited for dilute magnetic semiconductors (DMS), such as (In,Mn)As, (Ga,Mn)As, and $Mn_xGe_{1-x}$, where integration with semiconductor substrates, such as GaAs, follows naturally from the film growth process. In the DMS systems, the ferromagnetic interaction between the Mn spins (mediated by hole carriers) competes with the antiferromagnetic superexchange, and becomes dominant at sufficiently high hole doping Dietl et al. (2000). The demonstration of electric field modulation of magnetism in a 5 nm epitaxial (In,Mn)As layer was reported by Ohno et al. (2000), using a thick polyimide layer as the gate dielectric. By varying the charge carrier doping through the application of a gate voltage, a change in the critical temperature by about 2 K ($T_c = 25$ K at zero electric field) is achieved between the accumulation and depletion states. The size of the effect is found to agree with a Zener model used to describe the onset of magnetism in zinc-bled magnetic semiconductors Dietl et al. (2000). Besides (In,Mn)As Chiba et al. (2003); Ohno et al. (2000), electric field control of magnetism in magnetic semiconductors has been reported for $Mn_xGe_{1-x}$ Chen et al. (2007); Park et al. (2002); Xiu et al. (2010), (Zn,Mn)Se Kneip et al. (2006), and (Ga,Mn)As Chiba et al. (2008); Endo et al. (2010a); Nazmul et al. (2004); Owen et al. (2009); Riester et al. (2009); Stolichnov et al. (2008). In the report by Stolichnov et al. (2008), a ferroelectric polymer (polyvinylidene fluoride with trifluoroethylene, or P(VDF-TrFE)) is employed as the gate dielectric to achieve non-volatile control of ferromagnetism in a (Ga,Mn)As channel layer, as manifested by changes in the coercivity of the magnetic hysteresis loop and in the critical temperature as a function of the ferroelectric polarization direction.

### 2.2 Electrostatic control of magnetism in transition metals

The electrostatic control of magnetism in transition metals has been demonstrated by Weisheit et al. (2007), who report a modulation of the magnetic coercivity in ordered FePt and FePd intermetallic alloys subject to an applied field when immersed in an electrolyte. More recently, Maruyama et al. (2009) have shown that the perpendicular magnetic anisotropy of 2-4 monolayers (ML) Fe films can be modified by electric fields by using a polyimide layer as the gate dielectric (up to 40% for applied fields of the order of 1 MV/cm). The effect is particularly promising and could be explored to devise Fe/MgO/Fe magnetic tunnel junctions, where the tunnel magnetoresistance (TMR) is tuned electrostatically by controlling the magnetic anisotropy—and the relative magnetization alignment—of the Fe layers. Record high tunnel magnetoresistance ratios have been reported for Fe/MgO/Fe Bowen et al. (2001); Parkin et al. (2004); Yuasa et al. (2004), making this system a promising candidate for spintronic device applications. Indeed, control of the magnetic easy axis from in-plane to out of plane has been recently demonstrated for $Fe_{80}Co_{20}$ Shiota et al. (2009), while modulation of the magnetic anisotropy has been shown in $Fe_{80}Co_{20}$/MgO/Fe tunnel junctions Nozaki et al. (2010) and in MgO/$Co_{40}Fe_{40}B_{20}$/Ta structures Endo et al. (2010b). Another demonstration of electric field modulation of magnetism relies on the magnetic and structural instabilities of elemental Fe, where the application of an electric field is found to induce changes in the crystal structure of

Fe/Cu(111) islands, from the ferromagnetic bcc to the antiferromagnetic fcc structure Gerhard et al. (2010); first principles calculations show that the effect originates from changes in the Fe interatomic distances with the applied electric field as a result of electronic charge screening that tilts the energy of the system to favor a ferromagnetic or antiferromagnetic state Gerhard et al. (2010).

The theoretical study of the magnetoelectric coupling in metal-based multiferroic heterostructures has been the subject of intensive investigation. One can distinguish two approaches, one that considers the effect of charge screening in free standing metal layers subject to an external electric field, and the other that considers charge screening at the interface with a dielectric. In the latter case, contributions from chemical bonding between metal and dielectric need to be considered. The nature of the magnetoelectric effect that appears in metals can also be distinguished between enhanced spin imbalance at the Fermi level due to screening Zhang (1999), changes in the chemical bonding at the interface with the polarized dielectric, changes in the magnetic order with the charge density Gerhard et al. (2010); Kudasov & Korshunov (2007); Ovchinnikov & Wang (2008); Sun et al. (2010), and changes in the magnetic anisotropy Haraguchi et al. (2011); Maruyama et al. (2009); Nakamura et al. (2009); Niranjan et al. (2010); Tsujikawa & Oda (2009). The magnetoelectric effect of free standing metal films has been investigated for bcc Fe(001), fcc Ni(001), and hcp Co(0001) subject to a uniform electric field, where the charge screening induced spin-imbalance gives rise to surface magnetoelectric coupling coefficients of the order of $2-3\times10^{-14}$ Oe cm$^2$ V$^{-1}$ Duan et al. (2008), see Table 1. The magnetoelectric effect due to screening is enhanced in the presence of a dielectric due to the larger dielectric constant (compared to vacuum), in addition to effects induced by chemical bonding. For Fe/$BaTiO_3$(001), the results of density functional theory (DFT) calculations predict a large surface magnetoelectric response whose origin is largely attributed to changes in the chemical bonding at the interface, in particular, to hybridization between the Ti 3d, Fe 3d and O 2p orbital states, which is found to change significantly upon reversal of the ferroelectric polarization direction due to the displacement of the Ti atoms. The magnetoelectric coupling coefficient for 2 ML Fe/$BaTiO_3$ is estimated to be $\alpha = 0.01$ Oe cm V$^{-1}$ Duan et al. (2006) while for 1 ML Fe/$PbTiO_3$, $\alpha = 0.073$ Oe cm V$^{-1}$ Fechner et al. (2008); the effect of Fe oxidation has been predicted not to affect significantly the magnetoelectric coupling Fechner et al. (2009). In Fe/MgO(001), a surface magnetoelectric coupling $\alpha_s = 1.1\times10^{-13}$ Oe cm$^2$ V$^{-1}$ is found, significantly larger by a factor of 3.8 than that of a free standing Fe layer Niranjan et al. (2010); also in this system a linear change in the magnetocrystalline anisotropy with the applied electric field is reported. A different type of electric field control of magnetism consists of turning the magnetic state on and off; this approach has been investigated in the NiCu alloy at the composition corresponding to the boundary between magnetic and paramagnetic states. By capacitively charging the system, magnetic order can be modulated by effectively controlling the balance between the kinetic and exchange energies that determine the onset of magnetism Ovchinnikov & Wang (2008). The voltage sensitivity of ferromagnetic metallic systems near the critical temperature has also been studied in detail by the same authors Ovchinnikov & Wang (2009a;b). A related effect has been predicted for Pd, which is known to be a paramagnetic system with a Stoner parameter slightly short of fulfilling the condition for ferromagnetism by about 5-10%. First principles calculations suggest that depleting the Pd interface of charge carriers by means of an applied electric field can bring the Fermi level down and increase the density of states to favor an exchange-split (magnetic) state Kudasov & Korshunov (2007); Sun et al. (2010). A scheme for making the interfacial magnetoelectric effect additive consists of breaking the symmetry of ferromagnetic/dielectric bilayer structures by adding a non-magnetic metal at the other interface of the dielectric; this has been proposed by Cai et al. (2009), who have carried out

ab initio calculations for Fe, Co, Ni, $CrO_2/BaTiO_3/Pt$ systems to demonstrate this procedure (see Table 1). This approach ensures that spin accumulation at one interface is not canceled by depletion at the other interface and that the magnetoelectric response will increase linearly with the number of interfaces in a superlattice structure.

### 2.3 Electrostatic control of magnetism in complex oxides

The bulk of the experimental work aiming at controlling the magnetic state electrostatically in complex oxide materials has focused on the "colossal" magnetoresistive (CMR) manganites, which are characterized by rich magnetic and electronic phase diagrams as a function of chemical doping (see Section 3). In these compounds, the magnetic critical temperature is found to coincide approximately with a peak in the resistivity versus temperature curve, corresponding to a metal to insulator transition Urushibara et al. (1995). In turn, the temperature at which the resistivity peaks has been taken as a measure of the magnetic ordering temperature, providing a convenient, if indirect, method of probing the magnetic properties of thin films and device structures. Large changes in the resistivity peak temperature are observed in $Pb(Zr_{0.2}Ti_{0.8})O_3/La_{0.8}Sr_{0.2}MnO_3$ (PZT/LSMO) heterostructures, by 35 K for a 4.0 nm LSMO film Hong et al. (2003) and 50 K for a 3.8 nm LSMO film Hong et al. (2005); changes up to 43 K have also been reported for 7 u.c. $La_{0.7}Sr_{0.3}MnO_3$ side-gated channels Pallecchi et al. (2008); and for a 5 nm $La_{0.8}Ca_{0.2}MnO_3$/electrolyte field effect device, where a change of 32 K in the resistivity peak is observed between depletion and accumulation states. However, although closely related to the onset of magnetic order, the resistivity peak need not coincide with the magnetic critical temperature Bertacco et al. (2005); Lofland et al. (1997); indeed, a direct comparison between the resistivity and magnetization data in PZT/LSMO structures shows that while the peak in resistivity changes by 35 K between depletion and accumulation states, the critical temperature changes only by 20 K Vaz et al. (2010b). Direct measurements of the magnetic order parameter as a function of the applied electric field have been reported for PZT/10 nm $La_{0.85}Ba_{0.15}MnO_3$ Kanki et al. (2006), in PZT/4 nm $La_{0.8}Sr_{0.2}MnO_3$ Molegraaf et al. (2009); Vaz et al. (2010b) structures, and in 4-6 nm $La_{0.67}Sr_{0.33}MnO_3/SrTiO_3$ field effect device structures Brivio et al. (2010) using magnetooptic magnetometry. In the latter study, both top and bottom gated structures were investigated; the experimental results show that the critical temperature is modulated only for the top gated structure, i.e., for the structure where the screening occurs at the top LSMO interface Brivio et al. (2010). This result indicates that the properties of the bottom interface, characterized by the presence of an electric and magnetically "dead layer," is less amenable to field modulation. For the PZT/LBMO device structures Kanki et al. (2006), a change in the magnetic hysteresis loops is observed as the PZT polarization is switched, with the magnetic signal decreasing when going from the accumulation to the depletion state, a trend opposite to that found in the PZT/LSMO system Molegraaf et al. (2009); Vaz et al. (2010b), whose discussion we defer to Section 3.

The study of the magnetoelectric coupling in complex oxide heterostructures has also been carried out from the vantage point of first principles calculations. For $Fe_3O_4/BaTiO_3(001)$, a magnetoelectric response of $\alpha_s \sim 2 \times 10^{-10}$ Oe cm$^2$ V$^{-1}$ for $TiO_2$-terminated $BaTiO_3(001)$ is found Niranjan et al. (2008), comparable to the value obtained for $Fe/BaTiO_3$ Duan et al. (2006); the magnetoelectric effect in both these systems is attributed to changes in the bonding length of the Fe cations as a function of the direction of the ferroelectric polarization, giving rise to large changes in the magnetic moment of Fe. A magnetoelectric coupling based on charge screening and in the enhancement of the spin imbalance at the Fermi level has been studied in a symmetric $SrTiO_3/SrRuO_3/SrTiO_3$ structure, where the spin imbalance is described in terms of a spin capacitor effect, with the spin asymmetry stored at the interfaces

in a fashion similar to that of charge in a normal capacitor Rondinelli et al. (2008). A measure of the spin response of the interface is given in terms of the ratio of the surface spin polarization to the surface charge density, which is found to attain the value $\eta = 0.37$; this value remains the same when the $SrTiO_3$ is replaced by $BaTiO_3$, although the change in magnetic moment in the $SrRuO_3$ is much larger with $BaTiO_3$, a direct consequence of the larger amount of charge required to screen the ferroelectric polarization. The magnetoelectric response of $SrRuO_3/BaTiO_3(001)$ has also been studied, showing that, when subject to an electric field, the magnetic moment and the exchange splitting of $SrRuO_3$ are modified due to screening, resulting in a magnetoelectric coefficient $\alpha_s = 2.3 \times 10^{-10}$ Oe cm$^2$ V$^{-1}$ Niranjan et al. (2009). For half-metallic systems, the charge carrier density also determines the magnetic moment, and a simple argument shows that a universal magnetoelectric constant due to charge screening is expected, $\alpha_s = \mu_B/ec^2 \approx 6.44 \times 10^{-14}$ Oe cm$^2$ V$^{-1}$ Cai et al. (2009); Duan et al. (2009). A different magnetoelectric coupling mechanism is predicted theoretically in $La_{1-x}A_xMnO_3/BaTiO_3(001)$ ($A$ = Ca, Sr, or Ba) Burton & Tsymbal (2009), which relies on charge-induced modifications of the magnetic ground state of the CMR manganites Molegraaf et al. (2009). By choosing a doping level near the boundary between the ferromagnetic and antiferromagnetic state of $La_{1-x}A_xMnO_3$, the electrostatic doping arising from the ferroelectric polarization acts to favor either the ferromagnetic state (depletion state) or antiferromagnetic state (accumulation state), giving rise to a large change in the total magnetic moment for the two states of the ferroelectric polarization. This mechanism to magnetoelectric coupling had been suggested to occur in PZT/LSMO heterostructures Molegraaf et al. (2009) and will be discussed in more detail from an experimental perspective in the next section.

## 3. Magnetoelectric coupling in PZT/LSMO multiferroic heterostructures

The doped lanthanum manganites are complex oxides characterized by a strong interplay between charge, spin, and crystal lattice distortions, which is at the origin of the multifunctional behavior that is a hallmark of this class of compounds Moreo et al. (1999); Tokura & Tomioka (1999). Examples of the rich electronic and magnetic behavior found in the doped lanthanum manganites include magnetic and charge-ordered states, colossal magnetoresistance (CMR), high spin polarizations, and various electron transport regimes. The doped manganites crystallize in the pseudo-cubic $AMnO_3$ perovskite structure, where the 12-fold coordinated $A$-site cations are occupied by a large ion (e.g., alkaline and rare earths), while the Mn cations occupy octahedrally coordinated sites Johnsson & Lemmens (2007). Starting with the parent compound lanthanum manganite, $LaMnO_3$, where the Mn cations are in a trivalent state, the chemical substitution of La by a divalent alkaline earth removes the $e_g$ electron from the Mn cation, effectively adding a hole carrier to the system. The addition of carriers leads to profound modifications in the electronic and magnetic properties, resulting in complex phase diagrams as a function of chemical doping that include several electronic ground states Dagotto et al. (2001); Tokura (2006). This sensitivity to charge suggests that large susceptibilities to external electric fields can be attained when the system lies at the boundary separating two different ground states; by driving the system across the phase boundary using electrostatic doping, a change in the magnetic ground state of the system may be achieved. This approach has been explored in $PZT/La_{0.8}Sr_{0.2}MnO_3$ heterostructures, where the LSMO system is near the boundary separating insulating and metallic ferromagnetic ground states; large changes in the magnetic properties are expected by using the ferroelectric field effect approach to modulate the charge carrier doping of the LSMO film. For optimal use of the ferroelectric field effect, the channel layer thickness should be comparable to the screening

length Ahn et al. (2003); for LSMO ($x = 0.2$), with a charge carrier concentration of the order of $10^{21}$ cm$^{-3}$, the screening length has been estimated experimentally to be about 1 u.c. Hong et al. (2005). Hence, the growth of complex oxide field effect devices requires precise control of the thickness down to the unit cell level. Such fine control can be achieved with molecular beam epitaxy Vaz et al. (2010d) or pulsed laser deposition Huijben et al. (2008), where the film growth can be monitored layer-by-layer in real time by using the oscillations in the intensity of reflection high energy electron diffraction patterns. In the following, we provide an overview of the recent work demonstrating a large magnetoelectric coupling in PZT/LSMO heterostructures, as determined by probing directly the magnetic order parameter using local magnetooptic Kerr effect magnetometry Molegraaf et al. (2009). By using advanced spectroscopy techniques, we show that the observed effect is electronic in origin, and that it results from a change in the valence state of the Mn cations with the change in the hole carrier density Vaz et al. (2010b).

The sample structures consist of 250 nm $Pb(Zr_{0.2}Ti_{0.8})O_3/La_{0.8}Sr_{0.2}MnO_3/SrTiO_3(001)$, grown by a combination of molecular beam epitaxy for the LSMO film and off axis r.f. magnetron sputtering for the PZT layer. The LSMO film thickness is chosen to lie at the transition between the insulating and metallic states, typically 10-12 u.c. for $x = 0.2$ doping. The structures are single crystalline, with atomically flat and sharp interfaces Vaz et al. (2010d); PZT/LSMO films are deposited on both unpatterned and prepatterned $SrTiO_3(001)$ substrates; the latter consist of Hall bar device structures, defined prior to film deposition by optical lithography and with dimensions optimised for optical spectroscopy measurements Vaz et al. (2010d) (see Fig. 1(b), inset). A 10 nm Au gate electrode is then deposited onto the PZT layer, defining the active area of the device (i.e, the sample region where the PZT polarization is switched), using the LSMO layer as the bottom contact. The Au layer is chosen to be sufficiently thin to allow transmission of visible light for magnetooptic Kerr effect (MOKE) magnetometry measurements. MOKE relies on the fact that the polarization of light is modified upon reflection from a magnetic surface; it is a technique particularly well suited for this study, since it allows a direct and local measurement of the magnetic order parameter. In one implementation of this technique, a linearly polarized laser beam is reflected off the sample surface (with the plane of incidence parallel to the applied field direction, called the longitudinal MOKE geometry), and the Kerr rotation or ellipticity, which is proportional to the magnetization, is measured using a polarimeter unit Vaz et al. (2010e).

The individual electric and magnetic characteristics of the PZT/LSMO heterostructure are shown in Fig. 1(a) and (b), respectively. The electric polarization versus electric field (*P-E*) response shows abrupt electric switching and a saturation polarization of about 85 $\mu$C cm$^{-2}$; the magnetic hysteresis (*M-H*) curves, for both the accumulation and depletion states, show that the system is ferromagnetic at 100 K and that there is a marked difference in the magnetic properties for the two states of the ferroelectric polarization, namely, a larger coercivity and a smaller saturation magnetization for the accumulation state as compared to the depletion state. These individual ferroic curves are the classical hysteresis curves of ferroelectrics and ferromagnets; the magnetoelectric coupling is demonstrated by the magnetic response of the system as a function of the applied electric field (*M-E* loop) shown in Fig. 1(c), where the saturation magnetization is found to switch hysteretically and reversibly between a low and high magnetic moment at the electric field values corresponding to the switching of the ferroelectric polarization. This result demonstrates the presence of a magnetoelectric coupling in these multiferroic heterostructures, showing in particular that the direction of the PZT ferroelectric polarization modifies the magnetic state of the LSMO layer. Note that the difference in magnetic moment persists at zero applied electric field, which excludes electrostrictive or piezoelectric effects (strain) as being the cause of the observed

magnetoelectric effect. The magnetoelectric effect in the PZT/LSMO system is robust and has been observed in structures where the LSMO film has been grown by off axis magnetron sputtering Molegraaf et al. (2009) and molecular beam epitaxy Vaz et al. (2010b).

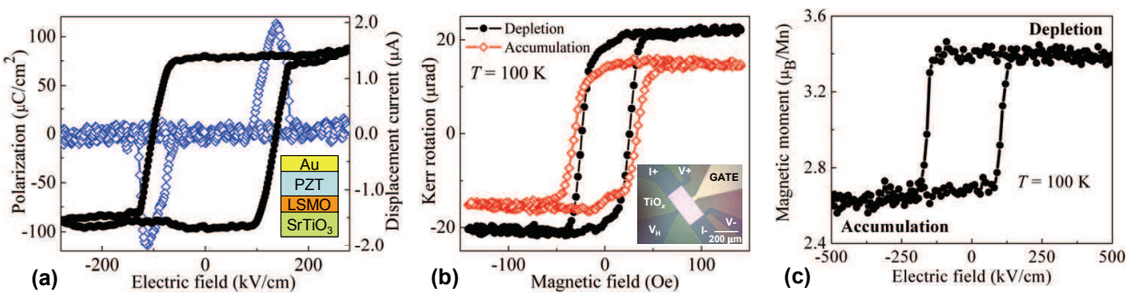


Fig. 1. Composite multiferroic heterostructure characterized by a coupling between the classical ferroelectric (a) and magnetic (b) ferroic responses, as shown in (c). While the *M-H* and *P-E* loops are standard, the *M-E* characteristic is new. The example shown is for a PZT/12 u.c. $La_{0.8}Sr_{0.2}MnO_3$ composite multiferroic heterostructure, from Vaz et al. (2010b; 2011). Figures (a) and (b): Copyright 2010 by The American Physical Society. Figure (c) reprinted with permission from C.A.F. Vaz et at., J. Appl. Phys., 109, 07D905 (2011). Copyright 2011, American Institute of Physics.

The variation of the magnetization as a function of temperature for the two states of the PZT polarization is shown in Fig. 2(a) Molegraaf et al. (2009); Vaz et al. (2010c). The magnetization curves are characteristic of a ferromagnetic system, with a critical temperature separating the high temperature paramagnetic regime and a ferromagnetically ordered state at low temperatures. What is striking in these data is that the direction of the PZT polarization determines the magnetic properties of the system, including an increase in the critical temperature (by about 20 K) and a decrease in the ground state magnetization when switching from the depletion to the accumulation state (in agreement with the *M-H* hysteresis curve of Fig. 1(b)). One sees that the state corresponding to the highest Curie temperature has the lowest saturation magnetization, which agrees qualitatively with what is expected from the behavior of bulk LSMO, since hole doping changes the ionic state of $Mn^{3+}$, with spin $S = 2$, to $Mn^{4+}$, with spin $S = 3/2$, so that we expect a decrease in magnetization with increasing doping Jonker & van Santen (1950).

As shown in Fig. 1(c), the magnetoelectric response of the PZT/LSMO multiferroic heterostructure is strongly non-linear, and the response of the system is best described in terms of an effective magnetoelectric susceptibility $\Delta M/\Delta E = \Delta M/2E_c$, where $E_c$ is the ferroelectric coercive field; at 100 K, we find $\Delta M/\Delta E = 6.2 \times 10^{-3}$ Oe cm $V^{-1}$. This value is significantly larger, by 2-3 orders of magnitude, than typical magnetoelectric coupling coefficients of single-phase multiferroics and comparable to the value obtained for strain-mediated composites Fiebig (2005); Ma et al. (2011); Vaz et al. (2010a). Given the interfacial nature of the magnetoelectric effect in this system, one alternate measure of the magnetoelectric effect is given in terms of the surface (interface) magnetoelectric coefficient $\alpha_s$, which is obtained by multiplying $\Delta M/2E_c$ by the LSMO film thickness, yielding $\alpha_s = 2.9 \times 10^{-9}$ Oe $cm^2$ $V^{-1}$ at 100 K. In Vaz et al. (2010c), the variation of the magnetoelectric response of PZT/LSMO as a function of the temperature is studied, as shown in Fig. 2(b). $\Delta M/2E_c$ is found to have a strong, non-monotonic, temperature variation, including a change in signal at around 150 K; in particular, one finds that the magnetoelectric response is largest at around 180 K, with $\Delta M/\Delta E = -13.5 \times 10^{-3}$ Oe cm $V^{-1}$ ($\alpha_s = -6.3 \times 10^{-9}$ Oe $cm^2$ $V^{-1}$),

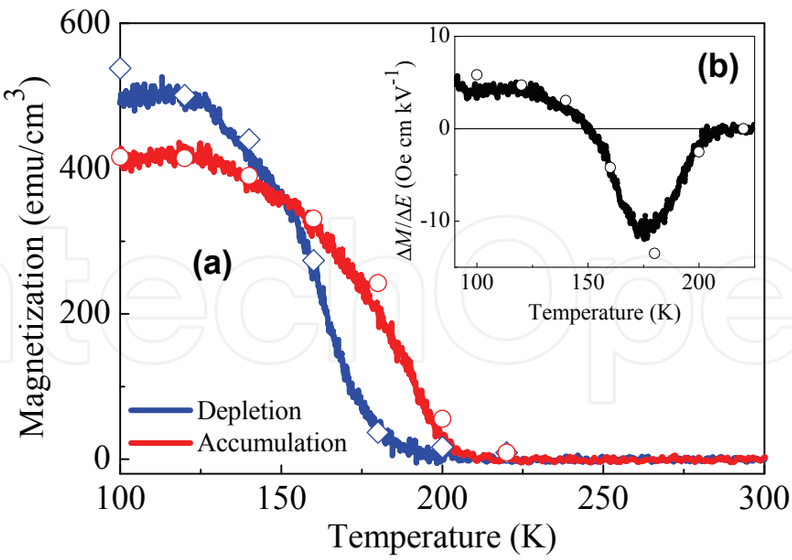


Fig. 2. (a) Magnetic response of the system as a function of temperature for the two states of the PZT polarization. (b) Variation in the magnetoelectric coupling coefficient $\Delta M/2E_c$ as a function of temperature. After Vaz et al. (2010c).

near the magnetic critical point, where the difference between the magnetization for the depletion and accumulation states is largest, as shown in Fig. 2(a). The change in sign of the magnetoelectric response can be understood with reference to the magnetization data shown in Fig. 2(a). One finds that 150 K separates a low temperature regime, where the magnetization for the depletion state is larger than that of the accumulation state, from a high temperature regime (up to the paramagnetic state), where the opposite behavior occurs due to the faster decay of the magnetization of the system in the depletion state on approaching its magnetic critical temperature. What is particularly promising in this system is that $\Delta M/\Delta E$ peaks at temperatures near the critical region, showing that the largest magnetoelectric response is achieved at the highest temperature where the system remains magnetic. A key aspect of composite multiferroics is that they need not obey reciprocity relations that limit the size of the magnetoelectric susceptibility in single phase compounds Brown et al. (1968).

The microscopic origin of the magnetoelectric effect is investigated by x-ray absorption near edge spectroscopy (XANES). XANES is a technique particularly well suited to study the changes in the electronic structure of Mn as a function of the applied electric field, due to its sensitivity to changes in the valence state. In XANES, one excites electrons from a core shell to empty states in the valence band (1s to 4p states for the case of the Mn $K$ edge). This excitation energy depends on the formal valence state of the cation, with the more electronegative cations requiring higher energy photons to excite core electrons Kirichok et al. (1985). One key advantage of x-ray absorption spectroscopy is its ability to probe buried layers, which is not possible with some other spectroscopic techniques, such as photoelectron spectroscopy. Details of the experimental set-up and measurement conditions are given in Vaz et al. (2010b;e).

The room temperature variation of the x-ray light absorption as a function of the incident photon energy across the absorption $K$ edge of Mn, for the depletion and accumulation states, is shown Fig. 3(a) Vaz et al. (2010b). The key result is the observation of an energy shift in the absorption edge of Mn between the depletion and accumulation states, by 0.3 eV, which corresponds to about 10% of the total shift expected for the full LSMO doping range Bindu

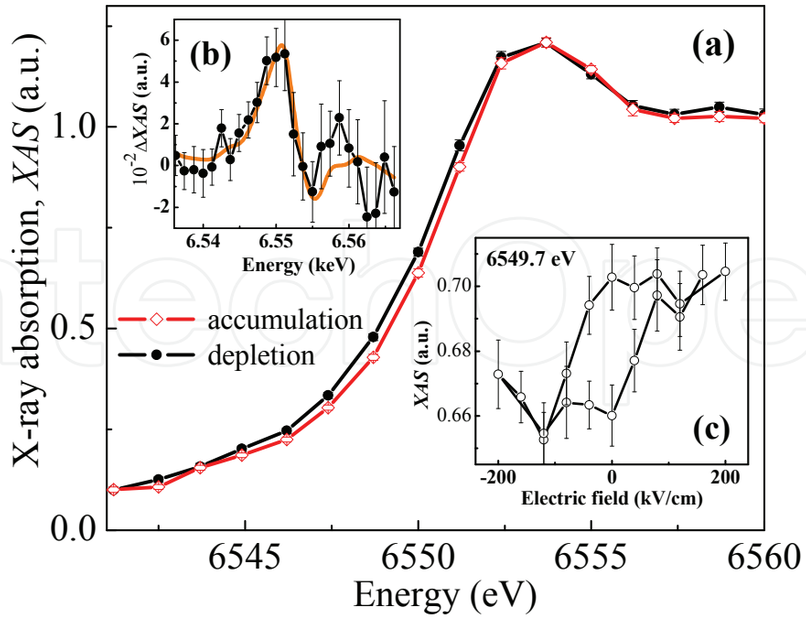


Fig. 3. (a) Room temperature XANES results for the two polarization states of the PZT. (b) Difference in x-ray absorption for the two PZT polarization states; the full line models this difference assuming a rigid shift in the Mn absorption edge. (c) Variation of the x-ray light absorption as a function of the applied gate voltage at a fixed energy, $E = 6549.7$ eV. The error bars reflect counting statistics. After Vaz et al. (2010b).

et al. (2005); Shibata et al. (2003). The shift in the absorption edge can also be observed in the difference x-ray absorption spectrum, shown in Fig. 3(b). The observation of a shift in the absorption $K$ edge of Mn shows that the valence state of Mn changes with charge doping induced by the ferroelectric polarization and demonstrates the electronic nature of the magnetoelectric coupling in these multiferroic heterostructures. The same result is observed at low temperature (20 K). From the observed energy shift we estimate the average change in valency across the LSMO film, $\Delta x = 0.1$ per Mn, using the results by Shibata et al. (2003) showing a linear variation in the energy shift with the formal average valency of Mn, $\Delta E = 3.0x$, where $x$ is the LSMO doping.

One can now compare the change in valency as determined by XANES with the values obtained from the electric and magnetic characterization of the same device structure. From the saturation electric polarization, $P_s = 85$ $\mu$C cm$^{-2}$, one can deduce the expected change in the carrier doping, $\Delta n = 0.13$ e/Mn. This value is in good agreement with the change in valency determined from XANES, $\Delta x = 0.1$ per Mn, showing that the electric polarization is screened effectively by hole carriers from the LSMO layer. Changing the valency of Mn from 3+ to 4+ leads to a change in spin state by 1/2 and to a change in magnetic moment of $gS \approx 1$ $\mu_B$ (where $g \approx 2$ is the $g$-factor), so one expects a change in the average magnetic moment of 0.1 $\mu_B$/Mn. However, from MOKE (Fig. 1(b)) in combination with SQUID magnetometry, one obtains a change in magnetic moment of about 0.76 $\mu_B$/Mn. This change is much larger than the expected change of 0.1 $\mu_B$/Mn from the change in spin state. One sees therefore that the change in magnetic moment cannot be explained simply by the change in the Mn spin state. From these results, and from the amplitude of the change in the magnetic moment, one concludes that a change in both the spin state and spin configuration must occur, whereby

the depletion state remains in a ferromagnetic state, while the accumulation state exhibits an antiferromagnetic configuration confined to the PZT interface where charge screening occurs. A model depicting the magnetic reordering is shown in Fig. 4. In this picture, the interface layer in the accumulation state consists of strongly depopulated 3d $z^2$ states, weakening the double-exchange interaction at these orbitals and favoring superexchange, leading to an antiferromagnetic coupling of the interfacial layer. This picture is in qualitative agreement with first principles calculations in strained LSMO Fang et al. (2000), and in particular with recent ab initio calculations by Burton and Tsymbal on $La_{1-x}Ba_xMnO_3/BaTiO_3$ Burton & Tsymbal (2009), where the low energy state of the system at $x = 0.5$ in the accumulation state corresponds to an antiparallel spin configuration of the interfacial spins. In this simplified model, the change in the interfacial spin configuration leads to a change in magnetic moment of about 0.6 $\mu_B$/Mn between depletion and accumulation states, which agrees with the experimental results. This mechanism gives rise to a much more dramatic change in the average magnetic moment and explains the large magnetoelectric coupling observed in this system. One direct consequence of these results is that one can control electrostatically both the spin state and magnetic spin configuration of the interfacial LSMO layer. Given that this layer is also responsible for charge transport, and given the high spin polarization characteristic of LSMO Park et al. (1998), this system constitutes a potential platform for the design of spintronics devices, such as lateral spin-valve structures, where the magnetic and transport properties are controlled by applied electric fields.

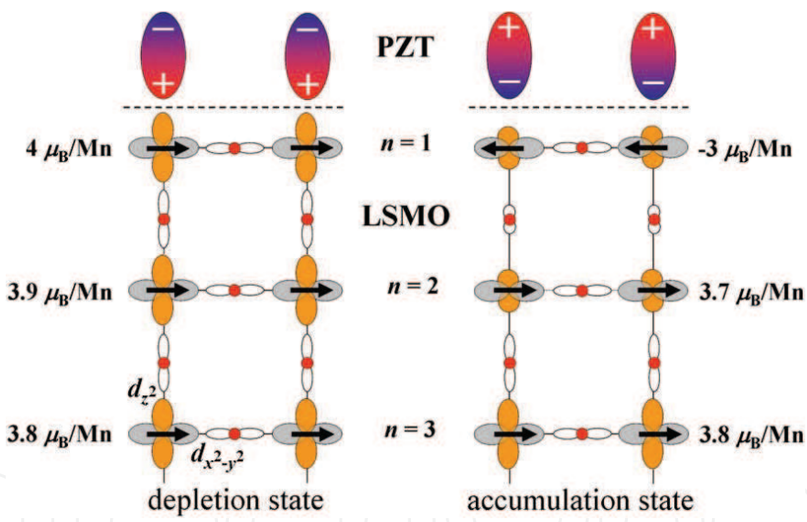


Fig. 4. Schematic model of the spin configurations in LSMO at the PZT interface for the depletion and accumulation states, showing the changes in the Mn and O orbital states and the expected changes in the magnetic moment per layer. The arrows indicate the spin orientation in the Mn cations and $n$ denotes the unit cell number below the PZT. The Mn $d$ orbitals are drawn in orange, and gray, and the lobes of the p orbitals are shown around the oxygen atoms (red). After Vaz et al. (2010b), Copyright 2010 by The American Physical Society.

## 4. Conclusion and outlook

To summarize, we illustrate how novel functionalities can be engineered by exploring the new phenomena that arise at the interface between dissimilar materials and how such

an approach can be used to achieve electrostatic control of magnetism in multiferroic heterostructures. By exploiting the sensitivity of the ground state properties of the CMR manganites to charge, we showed that large, charge-driven, magnetoelectric coupling in PZT/LSMO multiferroic heterostructures can be achieved. The effect is electronic in origin, as demonstrated by advanced spectroscopic techniques, and is therefore compatible with current CMOS technology, in particular since the growth of crystalline oxides on Si(001) is now well established McKee et al. (1998; 2001); Reiner et al. (2008). Further, we show that both the spin state and the magnetic configuration can be controlled electrostatically. One research challenge remains the optimization of the materials properties to allow room temperature operation; possible solutions are the use of optimal doping or the use of other magnetic oxides, such as the double perovskites. Another area that needs to be addressed is the dynamic magnetoelectric response of these multiferroic heterostructures, both in terms of the electric field modulation of the spin wave spectra and in terms of the electrostatic switching time of the magnetic state. Given that in these multiferroics the processes are electronically driven, one may expect very fast switching times, limited by the ferroelectric switching process. As this chapter aims to show, demonstrating the electrostatic switching of magnetism in a range of materials has been achieved as a proof of concept, and much remains to be investigated in terms of materials optimization, development and characterization of new systems, and understanding of the interfacial processes mediating the magnetoelectric coupling. The work achieved thus far illustrates how novel device structures enabling electric field control of the magnetic spin state can be tailored to provide the requisite characteristics that will make them potential candidates for next generation electronic devices.

## 5. Acknowledgments

This work supported by FENA, NSF 1006256, ONR, and from EU's Seventh Framework Programme IFOX (NMP3-LA-2010-246102). CAFV acknowledges M. Kläui for his continuing support.

## 6. References

Ahn, C. H., Bhattacharya, A., Ventra, M. D., Eckstein, J. N., Frisbie, C. D., Gershenson, M. E., Goldman, A. M., Inoue, I. H., Mannhart, J., Millis, A. J., Morpurgo, A. F., Natelson, D. & Triscone, J.-M. (2006). *Rev. Mod. Phys.* 78: 1185.

Ahn, C. H., Gariglio, S., Paruch, P., Tybell, T., Antognazza, L. & Triscone, J.-M. (1999). *Science* 284: 1152.

Ahn, C. H., Triscone, J.-M. & Mannhart, J. (2003). *Nature* 424: 1015.

Bertacco, R., Riva, M., Cantoni, M., Signorini, L. & Ciccacci, F. (2005). *Appl. Phys. Lett.* 86: 252502.

Bibes, M. & Barthélémy, A. (2007). *IEEE Trans. Electron Dev.* 54: 1003.

Bindu, R., Pandey, S. K., Kumar, A., Khalid, S. & Pimpale, A. V. (2005). *J. Phys.: Condens. Matter* 17: 6393.

Bowen, M., Cros, V., Petroff, F., Fert, A., Boubeta, C. M., Costa-Krämer, J. L., Anguita, J. V., Cebollada, A., Briones, F., de Teresa, J. M., Morellón, L., Ibarra, M. R., Güell, F., Peiró, F. & Cornet, A. (2001). *Appl. Phys. Lett.* 79: 1655.

Brivio, S., Cantoni, M., Petti, D. & Bertacco, R. (2010). *J. Appl. Phys.* 108: 113906.

Brown, Jr., W. F., Hornreich, R. M. & Shtrikman, S. (1968). *Phys. Rev.* 168: 574.

Brown, W. L. (1957). U.S. Patent 2,791,759.

Burton, J. D. & Tsymbal, E. Y. (2009). *Phys. Rev. B* 80: 174406.

Cai, T., Ju, S., Lee, J., Sai, N., Demkov, A. A., Niu, Q., Li, Z., Shi, J. & Wang, E. (2009). *Phys. Rev. B* 80: 140415(R).
Catalan, G. & Scott, J. F. (2009). *Adv. Mater.* 21: 2463.
Caviglia, A. D., Gariglio, S., Reyren, N., Jaccard, D., Schneider, T., Gabay, M., Thiel, S., Hammerl, G., Mannhart, J. & Triscone, J.-M. (2008). *Nature* 456: 624.
Cazayous, M., Gallais, Y., Sacuto, A., de Sousa, R., Lebeugle, D. & Colson, D. (2008). *Phys. Rev. Lett.* 101: 037601.
Chambers, S. A. (2010). *Adv. Mater.* 22: 219.
Chen, J., Wang, K. L. & Galatsis, K. (2007). *Appl. Phys. Lett.* 90: 012501.
Chiba, D., Sawicki, M., Nishitani, Y., Nakatani, Y., Matsukura, F. & Ohno, H. (2008). *Nature* 455: 515.
Chiba, D., Yamanouchi, M., Matsukura, F. & Ohno, H. (2003). *Science* 301: 943.
Chu, Y.-H., Martin, L. W., Holcomb, M. B., Gajek, M., Han, S.-J., He, Q., Balke, N., Yang, C.-H., Lee, D., Hu, W., Zhan, Q., Yang, P.-L., Fraile-Rodríguez, A., Scholl, A., Wang, S. X. & Ramesh, R. (2008). *Nature Mater.* 7: 478.
Cibert, J., Bobo, J.-F. & Lüders, U. (2005). *C. R. Physique* 6: 977.
Cohen, R. E. (2000). *J. Phys. Chem. Solids* 61: 139.
Dagotto, E., Hotta, T. & Moreo, A. (2001). *Phys. Rep.* 344: 1.
Dhoot, A. S., Israel, C., Moya, X., Mathur, N. D. & Friend, R. H. (2009). *Phys. Rev. Lett.* 102: 136402.
Dietl, T., Ohno, H., Matsukura, F., Cibert, J. & Ferrand, D. (2000). *Science* 287: 1019.
Duan, C.-G., Jaswal, S. S. & Tsymbal, E. (2006). *Phys. Rev. Lett.* 97: 047201.
Duan, C.-G., Nan, C.-W., Jaswal, S. S. & Tsymbal, E. Y. (2009). *Phys. Rev. B* 79: 140403(R).
Duan, C.-G., Velev, J. P., Sabirianov, R. F., Zhu, Z., Chu, J., Jaswal, S. S. & Tsymbal, E. (2008). *Phys. Rev. Lett.* 101: 137201.
Dzialoshinshkii, I. E. (1957). *Sov. Phys. JETP* 5: 1259.
Eckstein, J. N. & Bozovic, I. (1995). *Annu. Rev. Mater. Sci.* 25: 679.
Endo, M., Chiba, D., Shimotani, H., Matsukura, F., Iwasa, Y. & Ohno, H. (2010a). *Appl. Phys. Lett.* 96: 022515.
Endo, M., Kanai, S., Ikeda, S., Matsukura, F. & Ohno, H. (2010b). *Appl. Phys. Lett.* 96: 212503.
Fang, Z., Solovyev, I. V. & Terakura, K. (2000). *Phys. Rev. Lett.* 84: 3169.
Fechner, M., Maznichenko, I. V., Ostanin, S., Ernst, A., Henk, J., Bruno, P. & Mertig, I. (2008). *Phys. Rev. B* 78: 212406.
Fechner, M., Ostani, S. & Mertig, I. (2009). *Phys. Rev. B* 80: 094405.
Fennie, C. J. (2008). *Phys. Rev. Lett.* 100: 167203.
Fiebig, M. (2005). *J. Phys. D: Appl. Phys.* 38: R123.
Frey, T., Mannhart, J., Bednorz, J. G. & Williams, E. J. (1995). *Phys. Rev. B* 51: 3257.
Gerhard, L., Yamada, T. K., Balashov, T., Takács, A. F., Wesselink, R. J. H., Däne, M., Fechner, M., Ostanin, S., Ernst, A., Mertig, I. & Wulfhekel, W. (2010). *Nature Nanotechnology* 5: 792.
Haraguchi, S., Tsujikawa, M., Gotou, J. & Oda, T. (2011). *J. Phys. D: Appl. Phys.* 44: 064005.
Hehl, F. W., Obukhov, Y. N., Rivera, J.-P. & Schmid, H. (2008). *Phys. Rev. A* 77: 022106.
Hehl, F. W., Obukhov, Y. N., Rivera, J.-P. & Schmid, H. (2009). *Eur. Phys. J. B* 71: 321.
Hong, X., Posadas, A. & Ahn, C. H. (2005). *Appl. Phys. Lett.* 86: 142501.
Hong, X., Posadas, A., Lin, A. & Ahn, C. H. (2003). *Phys. Rev. B* 68: 134415.
Huijben, M., Martin, L. W., Chu, Y.-H., Holcomb, M. B., Yu, P., Rijnders, G., Blank, D. H. A. & Ramesh, R. (2008). *Phys. Rev. B* 78: 094413.
Imada, M., Fujimori, A. & Tokura, Y. (1998). *Rev. Mod. Phys.* 70: 1039.

Johnsson, M. & Lemmens, P. (2007). Crystallography and chemistry of perovskites, *in* H. Kronmüller & S. Parkin (eds), *Handbook of Magnetism and Advanced Magnetic Materials*, Vol. 4, John Wiley & Sons, p. 1.
Jonker, G. H. & van Santen, J. H. (1950). *Physica* 16: 337.
Kanki, T., Tanaka, H. & Kawai, T. (2006). *Appl. Phys. Lett.* 89: 242506.
Khomskii, D. I. (2006). *J. Magn. Magn. Mater.* 306: 1.
Khomskii, D. I. (2009). *Physics* 2: 20.
Kirichok, P. P., Kopaev, A. V. & Pashchenko, V. P. (1985). *Russian Physics Journal* 28: 849.
Kiselev, S. V., Ozerov, R. P. & Zhdanov, G. S. (1963). *Sov. Phys. — Doklady* 7: 742.
Kneip, M. K., Yakovlev, D. R., Bayer, M., Slobodskyy, T., Schmidt, G. & Molenkamp, L. W. (2006). *Appl. Phys. Lett.* 88: 212105.
Kudasov, Y. B. & Korshunov, A. S. (2007). *Phys. Lett. A* 364: 348.
Lebeugle, D., Colson, D., Forget, A. & Viret, M. (2007). *Appl. Phys. Lett.* 91: 022907.
Lebeugle, D., Colson, D., Forget, A., Viret, M., Bataille, A. M. & Gusakov, A. (2008). *Phys. Rev. Lett.* 100: 227602.
Lee, S., Ratcliff, W., Cheong, S.-W. & Kiryukhin, V. (2008). *Appl. Phys. Lett.* 92: 192906.
Lofland, S. E., Bhagat, S. M., Ghosh, K., Greene, R. L., Karabashev, S. G., Shulyatev, D. A., Arsenov, A. A. & Mukovskii, Y. (1997). *Phys. Rev. B* 56: 13705.
Looney, D. H. (1957). U.S. Patent 2,791,758.
Ma, J., Hu, J., Li, Z. & Nan, C.-W. (2011). *Adv. Mater.* 23: 9.
Martin, L. W., Chu, Y.-H. & Ramesh, R. (2010). *Materials Science and Engineering R* 68: 89.
Maruyama, T., Shiota, Y., Nozaki, T., Ohta, K., Toda, N., Mizuguchi, M., Tulapurkar, A. A., Shinjo, T., Shiraishi, M., Mizukami, S., Ando, Y. & Suzuki, Y. (2009). *Nature Nanotechnology* 4: 158.
McKee, R. A., Walker, F. J. & Chisholm, M. F. (1998). *Phys. Rev. Lett.* 81: 3014.
McKee, R. A., Walker, F. J. & Chisholm, M. F. (2001). *Science* 293: 468.
Miller, S. L. & McWhorter, P. J. (1992). *J. Appl. Phys.* 72: 5999.
Molegraaf, H. J. A., Hoffman, J., Vaz, C. A. F., Gariglio, S., van der Marel, D., Ahn, C. H. & Triscone, J.-M. (2009). *Adv. Mater.* 21: 3470.
Moreo, A., Yunoki, S. & Dagotto, E. (1999). *Science* 283: 2034.
Moriya, T. (1960). *Phys. Rev.* 120: 91.
Nakamura, K., Shimabukuro, R., Fujiwara, Y., Akiyama, T., Ito, T. & Freeman, A. J. (2009). *Phys. Rev. Lett.* 102: 187201.
Nan, C.-W., Bichurin, M. I., Dong, S., Viehland, D. & Srinivasan, G. (2008). *J. Appl. Phys.* 103: 031101.
Nazmul, A. M., Kobayashi, S., Sugahara, S. & Tanaka, M. (2004). *Physica E* 21: 937.
Neaton, J. B., Ederer, C., Waghmare, U. V., Spaldin, N. A. & Rabe, K. M. (2005). *Phys. Rev. B* 71: 014113.
Niranjan, M. K., Burton, J. D., Velev, J. P., Jaswal, S. S. & Tsymbal, E. Y. (2009). *Appl. Phys. Lett.* 95: 052501.
Niranjan, M. K., Duan, C.-G., Jaswal, S. S. & Tsymbal, E. Y. (2010). *Appl. Phys. Lett.* 96: 222504.
Niranjan, M. K., Velev, J. P., Duan, C.-G., Jaswal, S. S. & Tsymbal, E. Y. (2008). *Phys. Rev. B* 78: 104405.
Nozaki, T., Shiota, Y., Shinjo, T. & Suzuki, Y. (2010). *Appl. Phys. Lett.* 96: 022506.
Ohno, H., Chiba, D., Matsukura, F., Omiya, T., Abe, E., Dietl, T., Ohno, Y. & Ohtani, K. (2000). *Nature* 408: 944.
Ovchinnikov, I. V. & Wang, K. L. (2008). *Phys. Rev. B* 78: 012405.
Ovchinnikov, I. V. & Wang, K. L. (2009a). *Phys. Rev. B* 79: 020402(R).
Ovchinnikov, I. V. & Wang, K. L. (2009b). *Phys. Rev. B* 80: 012405.

Owen, M. H. S., Wunderlich, J., Novák, V., Olejník, K., Zemen, J., Výborný, K., Ogawa, S., Irvine, A. C., Ferguson, A. J., Sirringhaus, H. & Jungwirth, T. (2009). *New J. Phys.* 11: 023008.

Pallecchi, I., Pellegrino, L., Bellingeri, E., Siri, A. S., Marré, D., Tebano, A. & Balestrino, G. (2008). *Phys. Rev. B* 78: 024411.

Parendo, K. A., Tan, K. H. S. B., Bhattacharya, A., Eblen-Zayas, M., Staley, N. E. & Goldman, A. M. (2005). *Phys. Rev. Lett.* 94: 197004.

Park, J.-H., Vescovo, E., Kim, H.-J., Kwon, C., Ramesh, R. & Venkatesan, T. (1998). *Nature* 392: 794.

Park, Y. D., Hanbicki, A. T., Erwin, S. C., Hellberg, C. S., Sullivan, J. M., Mattson, J. E., Ambrose, T. F., Wilson, A., Spanos, G. & Jonker, B. T. (2002). *Science* 295: 651.

Park, Y.-G., Kanki, T., Lee, H.-Y., Tanaka, H. & Kawai, T. (2003). *Solid-State Electronics* 47: 2221.

Parkin, S. S. P., Kaiser, C., Panchula, A., Rice, P. M., Hughes, B., Samant, M. & Yang, S.-H. (2004). *Nature Mater.* 3: 862.

Picozzi, S. & Ederer, C. (2009). *J. Phys.: Condens. Matter* 21: 303201.

Posadas, A.-B., Lippmaa, M., Walker, F. J., Dawber, M., Ahn, C. H. & Triscone, J.-M. (2007). Growth and novel applications of epitaxial oxide thin films, *in* K. Rabe, C. H. Ahn & J.-M. Triscone (eds), *Physics of ferroelectrics*, Vol. 105 of *Topics in Applied Physics*, Springer-Verlag, p. 219.

R. E. Glover, I. & Sherrill, M. D. (1960). *Phys. Rev. Lett.* 5: 248.

Rabe, K. & Ghosez, P. (2007). First-principles studies of ferroelectric oxides, *in* K. Rabe, C. H. Ahn & J.-M. Triscone (eds), *Physics of ferroelectrics*, Vol. 105 of *Topics in Applied Physics*, Springer-Verlag.

Ramesh, R. & Spaldin, N. A. (2007). *Nature Mater.* 6: 21.

Ravindran, P., Vidya, R., Kjekshus, A., Fjellvåg, H. & Eriksson, O. (2006). *Phys. Rev. B* 74: 224412.

Reiner, J. W., Posadas, A., Wang, M., Ma, T. P. & Ahn, C. H. (2008). *Microelectronic Engineering* 85: 36.

Reiner, J. W., Walker, F. J. & Ahn, C. H. (2009). *Science* 323: 1018.

Riester, S. W. E., Stolichnov, I., Trodahl, H. J., Setter, N., Rushforth, A. W., Edmonds, K. W., Campion, R. P., Foxon, C. T., Gallagher, B. L. & Jungwirth, T. (2009). *Appl. Phys. Lett.* 94: 063504.

Rivera, J.-P. (1994). *Ferroelectrics* 161: 165.

Rondinelli, J. M., Stengel, M. & Spaldin, N. A. (2008). *Nature Nanotechnology* 3: 46.

Schlom, D. G., Haeni, J., Lettieri, J., Theis, C. D., Tian, W., Jiang, J. C. & Pan, X. Q. (1992). *Mater. Sci. Eng. B* 87: 282.

Shibata, T., Bunker, B. A. & Mitchell, J. F. (2003). *Phys. Rev. B* 68: 024103.

Shiota, Y., Maruyama, T., Nozaki, T., Shinjo, T., Shiraishi, M. & Suzuki, Y. (2009). *Appl. Phys. Express* 2: 063001.

Shvartsman, V. V., Kleemann, W., Haumont, R. & Kreisel, J. (2007). *Appl. Phys. Lett.* 90: 172115.

Sosnowska, I., Peterlin-Neumaier, T. & Steichele, E. (1982). *J. Phys. C: Sol. State Phys.* 15: 4835.

Spaldin, N. A. & Pickett, W. E. (2003). *J. Solid State Chem.* 176: 615.

Srinivasan, G. (2010). *Annu. Rev. Mater. Res.* 40: 153.

Stolichnov, I., Riester, S. W. E., Trodahl, H. J., Setter, N., Rushforth, A. W., Edmonds, K. W., Campion, R. P., Foxon, C. T., Gallagher, B. L. & Jungwirth, T. (2008). *Nature Mater.* 7: 464.

Sun, Y., Burton, J. D. & Tsymbal, E. Y. (2010). *Phys. Rev. B* 81: 064413.

Talyansky, V., Ogale, S. B., Takeuchi, I., Doughty, C. & Venkatesan, T. (1996). *Phys. Rev. B* 53: 14575.

Thiele, C., Dörr, K., Bilani, O., Rödel, J. & Schultz, L. (2007). *Phys. Rev. B* 75: 054408.
Tokura, Y. (2006). *Rep. Prog. Phys.* 69: 797.
Tokura, Y. & Nagaosa, N. (2000). *Science* 288: 462.
Tokura, Y. & Tomioka, Y. (1999). *J. Magn. Magn. Mater.* 200: 1.
Tsujikawa, M. & Oda, T. (2009). *Phys. Rev. Lett.* 102: 247203.
Urushibara, A., Moritomo, Y., Arima, T., Asamitsu, A., Kido, G. & Tokura, Y. (1995). *Phys. Rev. B* 51: 14103.
van Suchtelen, J. (1972). *Philips Res. Repts* 27: 28.
Vaz, C. A. F., Wang, H.-Q., Ahn, C. H., Henrich, V. E., Baykara, M. Z., Schwendemann, T. C., Pilet, N., Albers, B. J., Schwarz, U., Zhang, L. H., Zhu, Y., Wang, J. & Altman, E. I. (2009a). *Surf. Sci.* 603: 291.
Vaz, C. A. F., Hoffman, J., Posadas, A.-B. & Ahn, C. H. (2009b). *Appl. Phys. Lett.* 94: 022504.
Vaz, C. A. F., Hoffman, J., Ahn, C. H. & Ramesh, R. (2010a). *Adv. Mater.* 22: 2900.
Vaz, C. A. F., Hoffman, J., Segal, Y., Reiner, J. W., Grober, R. D., Zhang, Z., Ahn, C. H. & Walker, F. J. (2010b). *Phys. Rev. Lett.* 104: 127202.
Vaz, C. A. F., Segal, Y., Hoffman, J., Grober, R. D., Walker, F. J. & Ahn, C. H. (2010c). *Appl. Phys. Lett.* 97: 042506.
Vaz, C. A. F., Segal, Y., Hoffman, J., Walker, F. J. & Ahn, C. H. (2010d). *J. Vac. Sci. Technol. B* 28: C5A6.
Vaz, C. A. F., Hoffman, J., Segal, Y., Walker, F. J. & Ahn, C. H. (2010e). *Proc. of SPIE* 7760: 776013.
Vaz, C. A. F., Hoffman, J., Segal, Y., Marshall, M. S. J., Reiner, J. W., Grober, R. D., Zhang, Z., Walker, F. J. & Ahn, C. H. (2011). *J. Appl. Phys.* 109: 07D905.
Venkatesan, T., Kundaliya, D. C., Wu, T. & Ogale, S. B. (2007). *Phil. Mag. Lett.* 87: 279.
Vrejoiu, I., Alexe, M., Hesse, D. & Gösele, U. (2008). *Adv. Mater.* 18: 3892.
Waghmare, U. V. & Rabe, K. M. (2005). Dielectric properties of simple and complex oxides from first principles, *in* A. A. Demkov & A. Navrotsky (eds), *Materials Fundamentals of Gate Dielectrics*, Springer, Dordrecht, p. 215.
Wang, J., Neaton, J. B., Zheng, H., Nagarajan, V., Ogale, S. B., Liu, B., Viehland, D., Vaithyanathan, V., Schlom, D. G., Waghmare, U. V., Spaldin, N. A., Rabe, K. M., Wuttig, M. & Ramesh, R. (2003). *Science* 299: 1719.
Wang, K. F., Liu, J. M. & Ren, Z. F. (2009). *Adv. Phys.* 58: 321.
Weisheit, M., Fähler, S., Marty, A., Souche, Y., Poinsignon, C. & Givord, D. (2007). *Science* 315: 349.
Wu, S. M., Cybart, S. A., Yu, P., Rossell, M. D., Zhang, J. X., Ramesh, R. & Dynes, R. C. (2010). *Nature Mater.* 9: 756.
Xiu, F., Wang, Y., Kim, J., Hong, A., Tang, J., Jacob, A. P., Zou, J. & Wang, K. L. (2010). *Nature Materials* 9: 337.
Yuasa, S., Nagahama, T., Fukushima, A., Suzuki, Y. & Ando, K. (2004). *Nature Mater.* 3: 868.
Zhang, S. (1999). *Phys. Rev. Lett.* 83: 640.
Zheng, H., Straub, F., Zhan, Q., Yang, P.-L., Hsieh, W.-K., Zavaliche, F., Chu, Y.-H., Dahmen, U. & Ramesh, R. (2006). *Adv. Mater.* 18: 2747.
Zhu, Y. (ed.) (2005). *Modern techniques for characterizing magnetic materials*, Kluwer Academic Publishers, Boston.
Zubko, P., Gariglio, S., Gabay, M., Ghosez, P. & Triscone, J.-M. (2011). *Ann. Rev. Condens. Matter Phys.* 2: 141.
Žutić, I., Fabian, J. & Das Sarma, S. (2004). *Rev. Mod. Phys.* 76: 323.

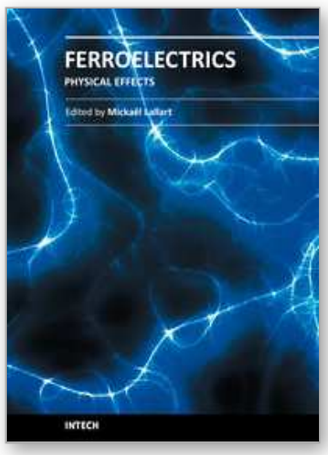


**Ferroelectrics - Physical Effects**

Edited by Dr. MickaÃ«l Lallart

ISBN 978-953-307-453-5
Hard cover, 654 pages
**Publisher** InTech
**Published online** 23, August, 2011
**Published in print edition** August, 2011

Ferroelectric materials have been and still are widely used in many applications, that have moved from sonar towards breakthrough technologies such as memories or optical devices. This book is a part of a four volume collection (covering material aspects, physical effects, characterization and modeling, and applications) and focuses on the underlying mechanisms of ferroelectric materials, including general ferroelectric effect, piezoelectricity, optical properties, and multiferroic and magnetoelectric devices. The aim of this book is to provide an up-to-date review of recent scientific findings and recent advances in the field of ferroelectric systems, allowing a deep understanding of the physical aspect of ferroelectricity.



INTECH
open science | open minds

**InTech Europe**
University Campus STeP Ri
Slavka Krautzeka 83/A
51000 Rijeka, Croatia
Phone: +385 (51) 770 447
Fax: +385 (51) 686 166
www.intechopen.com

**InTech China**
Unit 405, Office Block, Hotel Equatorial Shanghai
No.65, Yan An Road (West), Shanghai, 200040, China
中国上海市延安西路65号上海国际贵都大饭店办公楼405单元
Phone: +86-21-62489820
Fax: +86-21-62489821

IntechOpen